High Conductivity Electrode using Oxalic Acid-doped Polyaniline for Vanadium Redox Flow Battery

Hairul Mardiah Hamzah[1], Sabrina M Yahaya[1], Muhd Zu Azhan Yahya[2] and Amirah Amalina Ahmad Tarmizi[1]*

[1]Faculty of Applied Science, Universiti Teknologi MARA, Shah Alam, 40450 Shah Alam, Selangor, Malaysia

[2]Faculty of Defence Science and Technology, Universiti Pertahanan Nasional Malaysia, 57000 Kuala Lumpur, Malaysia

*Corresponding author (e-mail: amirahamalina@uitm.edu.my)

The increasing global demand for sustainable energy storage solutions has driven advancements in vanadium redox flow batteries (VRFBs). However, the low power density of VRFBs remains a critical challenge due to the limited electrochemical performance of conventional graphite felt (GF) electrodes. In this study, polyaniline (PANI) doped with oxalic acid was synthesized via oxidative polymerization and used to modify GF electrodes to enhance their conductivity and electrochemical activity. Structural and morphological characterizations, including FTIR and FESEM-EDX, suggested the successful incorporation of PANI onto the GF surface, significantly improving the electrode's porosity and active surface area. The modified electrode demonstrated a fivefold reduction in charge transfer resistance (Rct) and a substantial increase in electrical conductivity (from 0.0043 S/cm to 0.0214 S/cm), when analysed by electrochemical impedance spectroscopy (EIS). Cyclic voltammetry (CV) results revealed enhanced redox kinetics and pseudocapacitive behavior, enabling superior charge storage capability and improved ion transport, with a specific capacitance of 125 F g^{-1} at 10 mV s^{-1}. Additionally, the modified electrode delivered a power density of 178.5 W g^{-1}, indicating excellent energy transfer capability. These findings highlight that oxalic acid-doped PANI is a cost-effective and scalable electrode modification approach, paving the way for high-performance VRFBs and other energy storage applications.

Keywords: Polyaniline; oxalic acid; graphite felt,VRFBs; EIS; CV

Received: March 2025; Accepted: June 2025

Despite global attempts to reach carbon peaking and carbon neutrality targets, the contemporary industry faces the dual constraints of fossil fuel: resource depletion and environmental degradation. The primary objective is to encourage the transition of energy composition worldwide, aiming to replace fossil fuels with renewable and environmentally friendly energy sources [1]. Conventional renewable energy sources, such as wind, solar, and tidal energy, are currently demonstrating significant promise. Nevertheless, the irregularity and unpredictability of their occurrence create difficulties for energy systems. Hence, the development of large-scale energy storage devices is necessary to achieve widespread implementation of renewable energy and facilitate the transition to sustainable energy sources [2].

The vanadium redox flow battery (VRFB) was initially proposed in 1985 by the Skyllas-Kazacos team. The researchers then did an in-depth investigation on altering VRFB electrode materials[3, 4]. Figure 1 shows a schematic representation of VRFB. VRFB consists primarily of electrodes, an ion exchange membrane, and an electrolyte.

The principal active ingredient in the system is the vanadium ion, which may exist in various valence states. After being energized, the current is imported and exported via the collector. The electrolyte solution performs a redox reaction on the electrode surface, which allows the battery to be charged and discharged. When the battery is charged, the negative electrolyte's V^{3+} concentration is lowered to V^{2+}. The VO^{2+} in the positive electrolyte loses electrons and oxidizes into VO_2^+. The oxidation and reduction reactions of the vanadium electrolyte are shown in equations 1-3 below, with their respective potentials.

Positive half-cell:

$$VO^{2+} + H_2O \rightleftharpoons VO_2^+ + 2H^+ + e^- \qquad E^o = 1.00\ V \qquad (1)$$

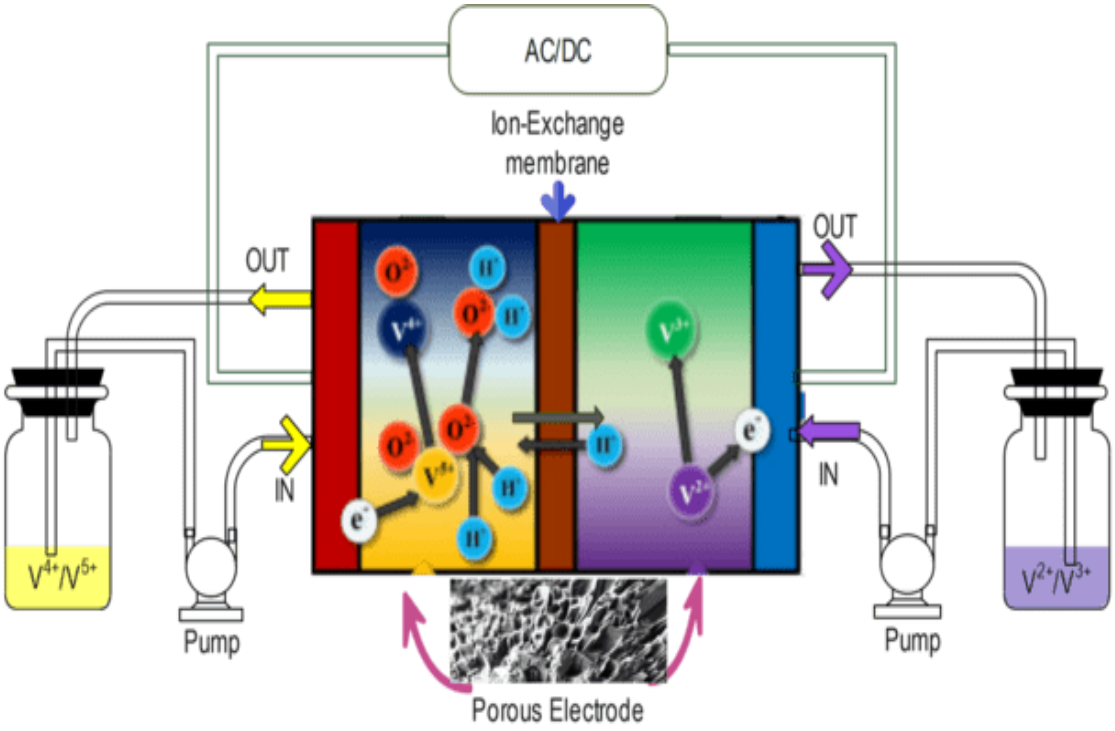

Figure 1. Illustration of a vanadium redox flow battery.

Negative half-cell:

$$VO^{3+} + e^{-} \rightleftharpoons V^{2+} \qquad E^{o}= -0.26\ V \qquad (2)$$

Overall equation:

$$VO^{2+} + H_2O + V^{3+} \rightleftharpoons VO_2^{+} + V^{2+} + 2H^{+} \qquad E^{o}= 1.26\ V \qquad (3)$$

The electrode, as a fundamental element of the battery, plays a pivotal role in influencing the performance of the VRFB as it not only offers active sites for redox reactions but also impacts mass and ion movement [5]. Currently, the carbon material graphite felt (GF) has been used as an electrode for VRFB due to its strength, high surface area, wide range operating potential, acid resistance, and high conductivity [6, 7]. Unfortunately, GF has poor hydrophilicity and low kinetic reversibility, and needs to be treated for better cyclability and wettability [7]. Several surface treatments have been developed to raise the electrochemical activity of the electrode to increase the number of oxygen functional groups or nitrogen functional groups. These include thermal treatment, salt treatment, acid treatment, ammonia treatment, or depositing catalysts onto the surface of the electrode[4, 8-14]. Recently, conducting materials have been used to enhance the properties of the electrode in energy storage applications such as supercapacitors, lithium-ion batteries, fuel cells, and redox flow batteries[15-17].

Polyaniline (PANI) is a versatile conducting material used in many applications such as supercapacitors, solar cells, sensors, organic light-emitting diodes (OLEDs), anticorrosion, wound healing, nanomedicine, and tissue engineering. PANI was chosen as the conducting material due to its low price, ease of synthesis, low toxicity, and high electrical conductivity [18, 19]. A conducting polyaniline can be synthesised by reacting a Lewis base aniline monomer with a Bronsted acid. This reaction produces an anilinium salt, and with the aid of an oxidant, the salt may be converted from an emeraldine base to an emeraldine salt that is neutralized and partially oxidized. Polyaniline contains two aromatic backbones, a quinonoid and a benzenoid. The structure of the benzenoid and quinonoid rings in a polyaniline backbone is illustrated in Figure 2.

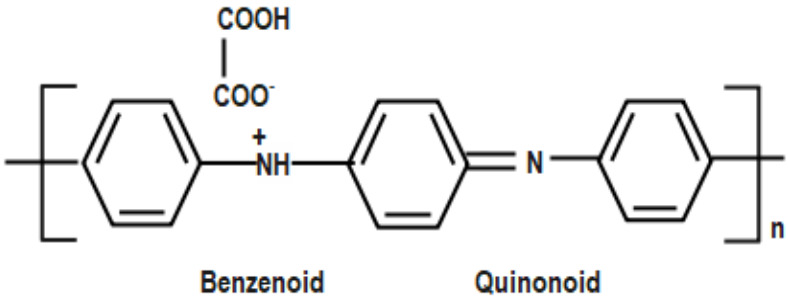

Figure 2. Structure of benzenoid and quinonoid rings in a polyaniline backbone.

The PANI incorporated with nano-titanium carbide was coated on the GF and employed as an electrode in the VRFB, which produced 98.89 % Coulombic efficiency and good stability [18]. The negative half-cell limited the electrochemical performance of the VRFB because of the competitive hydrogen evolution reaction, leading to the slow reaction kinetics of V^{3+}/V^{2+}. A PANI/graphene oxide composite was used in another study to modify the GF via electrodeposition for bio-electrochemical systems, and this achieved a higher maximum power density [20]. In this work, PANI doped with oxalic acid was polymerized onto the surface of the GF via oxidative polymerization. The modified GF with oxalic acid-doped PANI served as the VRFB electrode. The suitability of oxalic acid as a dopant for GF-PANI was investigated via the supercapacitor properties of the electrode in the energy storage system.

EXPERIMENTAL

Chemicals and Materials

The reagents used were aniline (Sigma Aldrich), oxalic acid (Chemiz), ammonium persulfate (Chemiz), commercial graphite felt (PAN-based GF, 5mm thickness), methanol, and distilled water.

Methods and Characterization

The oxalic acid-doped polyaniline was embedded into the surface of GF by oxidative polymerization using ammonium persulfate as the oxidant. Aniline monomer was dissolved in 50 mL 0.1 M HCl and mixed with 450 mL oxalic acid, the dopant. The mixture was stirred for 6 hours in an ice bath and left aging overnight in a chiller.

FT-IR spectra (4000-500 cm^{-1}) of aniline and oxalic acid-doped PANI were obtained with a Bruker Alpha Platinum ATR-FTIR spectrometer. Field emission scanning electron microscopy (FESEM) and energy-dispersive X-ray (EDX) spectroscopy were used to observe the morphology and elemental analysis of oxalic acid-doped PANI, GF modified with polyaniline, and carbonized GF modified with polyaniline.

The specific surface area and pore characteristics of the samples were analysed using nitrogen adsorption-desorption isotherms at 77 K with a surface area and porosity analyser. Prior to the measurements, all samples were degassed under vacuum at an elevated temperature to remove adsorbed gases or moisture. The Brunauer-Emmett-Teller (BET) method was employed to calculate the specific surface area based on the nitrogen adsorption data in the relative pressure range of $P/P_o = 0.05\text{-}0.30$.

The conductivity of these samples was assessed through electrochemical impedance spectroscopy (EIS) utilizing the Gamry EIS 620 Potentiostat. To ascertain the electrical properties of PANI, impedance measurements were conducted by placing the sample between two stainless steel electrodes with an area of 1 cm^2. Impedance measurements were conducted across a frequency range from 100 MHz to 0.1 Hz, utilizing a sinusoidal wave of 10 mV at ambient temperature. The electrode's conductivity was determined using the bulk resistance (R_b) value obtained from the Nyquist plot. The proton conductivity was calculated using Equation (4):

$$\sigma = \frac{L(cm)}{A(R_b)} \quad (4)$$

Where R_b (Ω) is the resistance of the sample and L(cm) and A (cm^2) are the thickness and area of the electrode, respectively.

Cyclic voltammetry from a three-electrode system was used to collect redox potential and electrochemical reversibility data. The system utilized a graphite rod as a counter electrode, Ag/AgCl as the reference electrode, and GF-PANI as the working electrode. The working electrode (1 cm x 1 cm) was attached to a crocodile clip and immersed in 1 M H_2SO_4.

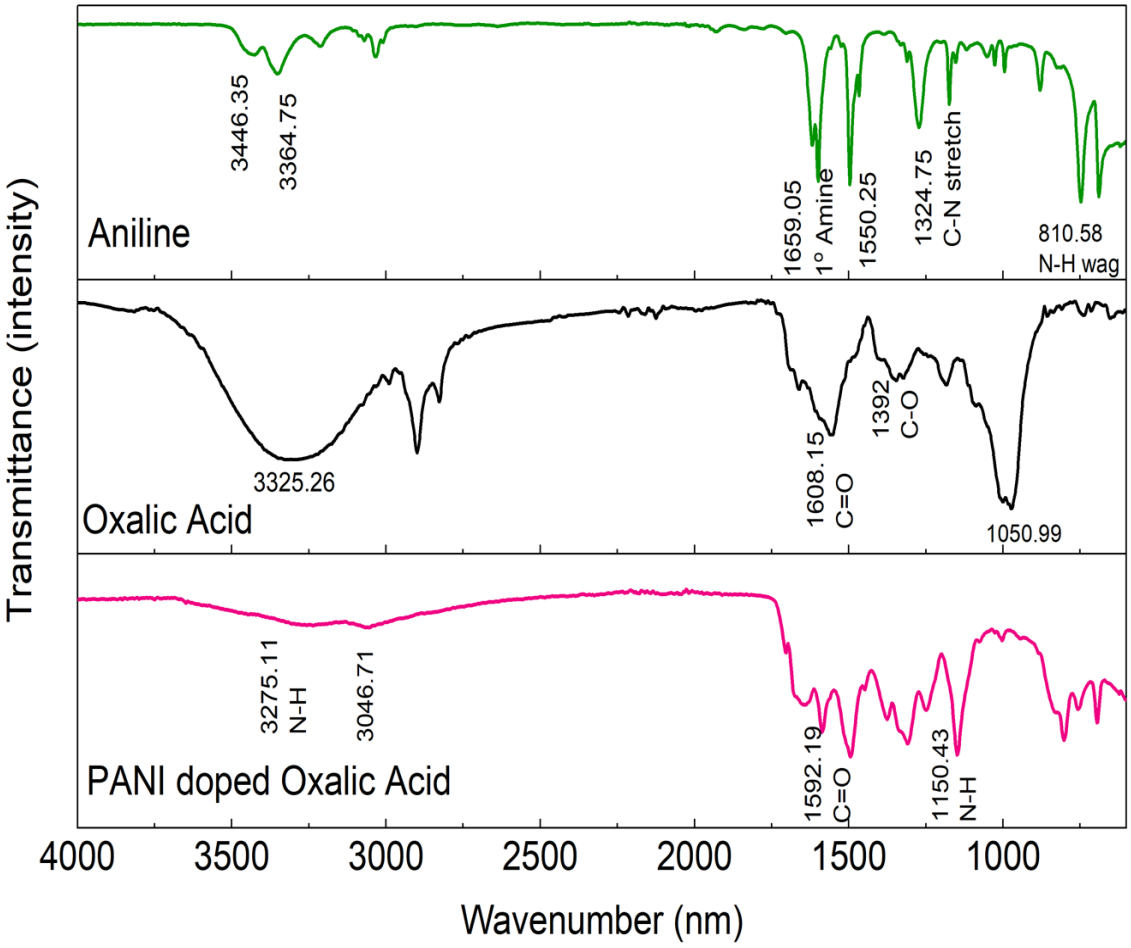

Figure 3. FTIR spectra of aniline monomer, oxalic acid, and polyaniline doped with oxalic acid (0.08 M).

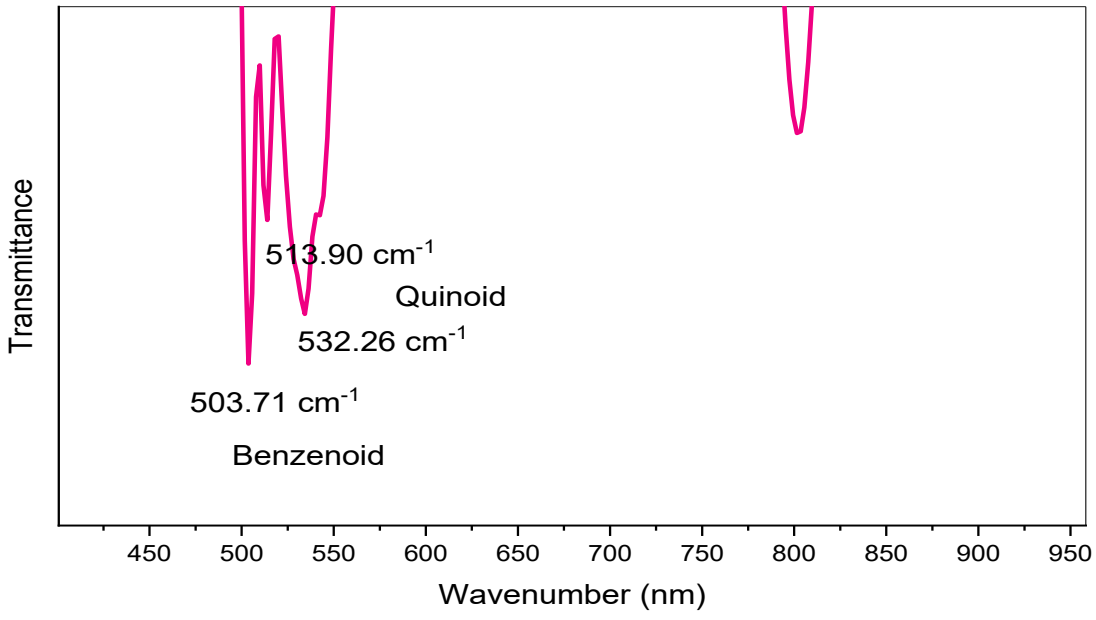

Figure 4. FTIR spectrum of polyaniline with 0.08 M oxalic acid, enlarged at the 450 cm^{-1} – 900 cm^{-1} region.

The peaks observed in a cyclic voltammogram are a result of the Nernst equation, which connects the potential of the electrochemical cell to the standard potential of the electroactive species and the relative concentrations of its oxidized and reduced components at equilibrium. During a cyclic voltammetry experiment, the potential scan leads to variations in species concentration at the electrode surface, following the principles outlined in the Nernst Equation below.

$$E = E^{o} - \frac{RT}{zF} \ln Q \quad (5)$$

E represents the reduction potential, E^0 denotes the standard potential, R signifies the universal gas constant, T indicates the temperature in Kelvin, z refers to the ion charge (moles of electrons), F stands for the Faraday constant, and Q is the reaction quotient.

RESULTS AND DISCUSSION

The conversion of aniline to polyaniline was analyzed by FTIR. Figure 3 depicts the infrared spectra of the aniline monomer, oxalic acid, and polyaniline-doped oxalic acid samples. The FTIR spectra indicate that on oxidation of aniline to polyaniline, utilizing oxalic acid as a dopant, the polyaniline backbone was an emeraldine salt. The spectrum of polymerised polyaniline (PANI) demonstrated notable absorption peaks for C=N, such as the imine peak at 1625.32 cm^{-1}. It also revealed peaks at 3046.71 and 3275.11 cm^{-1} for N-H stretching and C-H stretching of the aliphatic chain. A band at 1152.20 cm^{-1} was attributed to the vibration mode of $–NH^{+}=$, linked to the vibrations of the charged polymer quinonoid structure. This suggests that positive charges were present on the polymer chain [21]. The absorption band at 1303.11 cm^{-1} in the polyaniline spectrum is associated with π-electron delocalization in the polymer, induced by C–H out-of-plane bending vibrations, corresponding to a peak at 813 cm^{-1}. In Figure 4, the quinonoid ring peak appeared at 513.90 and 532.26 cm^{-1} for aromatic C-H out-of-plane bending, while para-C-H out-of-plane bending was observed at 813.69 cm^{-1}. The aromatic C-H peak of the benzenoid ring was present at 503.71 cm^{-1}.

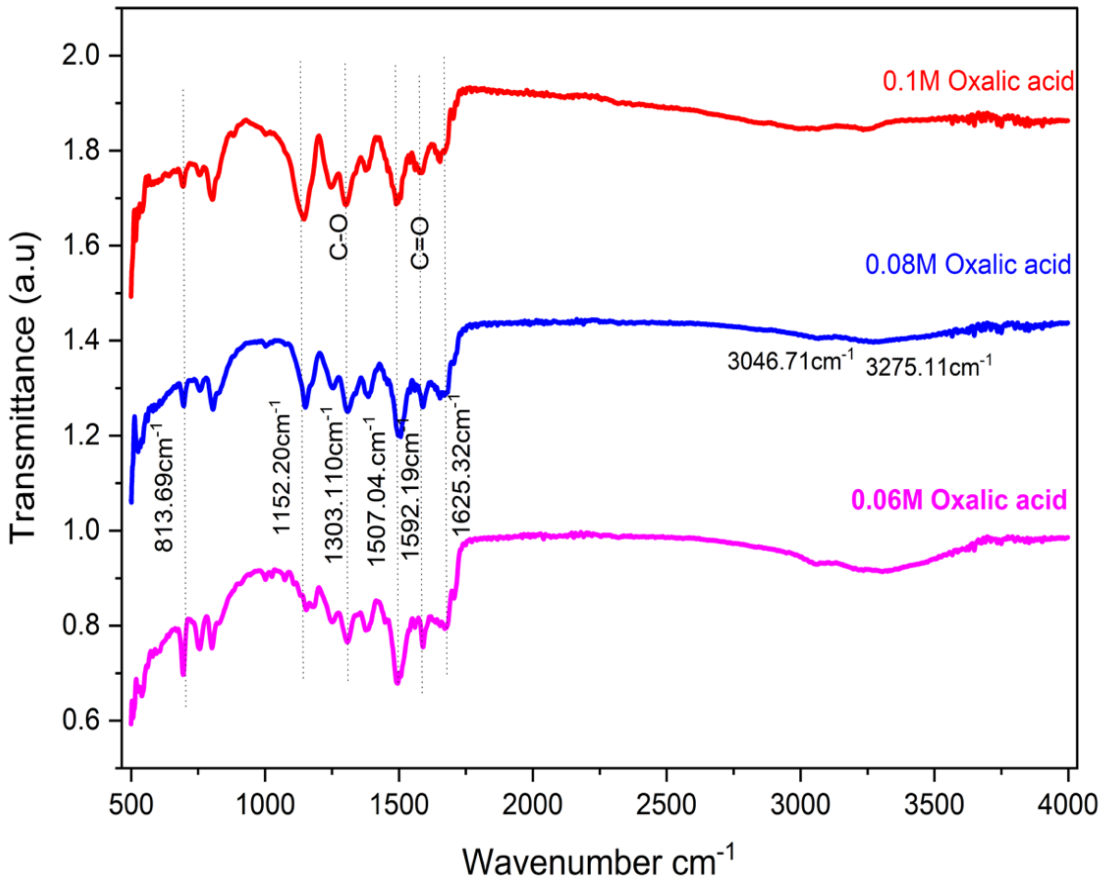

Figure 5. FTIR spectra of polyaniline doped with 0.06 M, 0.08 M, and 0.1 M oxalic acid.

Table 1. Analysis of the FTIR spectrum for polyaniline.

Wavenumber range (cm^{-1})	Expected vibration
513.90, 532.26	Aromatic C-H out of plane bending (quinoid)
503.71	Aromatic C-H (benzenoid)
691.50	Aromatic C-H out-of-plane bending
813.69	Para C-H out-of-plane bending (quinoid)
1152.20	N-H vibration
1303.07	C-N stretching of secondary aromatic ring
1488.69, 1507.04	C=C stretch in aromatic ring
1625.32	C=N from imine
3046.71, 3275.11	N-H stretching vibrations of 2nd amine

The increase in the oxalic acid dopant concentration can be seen from the FTIR spectra in Figure 5. Four peaks are associated with aromatic C-H out-of-plane bending at 691.50 cm^{-1}, the -NH^{+}= vibrations at 1152.20 cm^{-1}, and C=N from imine vibrations at 1625.32 cm^{-1}. These peaks can be differentiated from each other. The intensity of the C-H out-of-plane bending peak decreased with the increase in oxalic acid concentration from 0.06 M to 0.1 M. This information provides us with the ring's substitution patterns. A strong peak is associated with mono-substitution of the aromatic ring. A similar result was found in the formation of a PANI nanocomposite for chronic diseases [22]. From this experiment, it was suggested that 0.06 M oxalic acid did not fully attach oxalic acid to the backbone as a dopant. This might be due to fewer oxalate anions being available to protonate the PANI, which lead to incomplete or weaker attachment of the dopant to the backbone. A study by Ahmad Tarmizi et al. investigated the effect of varying oxalic acid concentrations on the electrical properties of PANI. They found that doping PANI with 0.1 M oxalic acid resulted in the highest conductivity, while both lower and higher concentrations led to decreased conductivity [23]. This suggests that an optimal concentration of oxalic acid is necessary to achieve effective integration with the PANI backbone. The ideal structure for polyaniline and the dopant was para-substitution of partially oxidized quinonoid rings and benzenoid rings, as can be seen in Figure 2. At 0.08 M and 0.1 M concentrations of oxalic acid, the -NH^{+}= peak appeared to be strong. The C=N imine peak also appeared with 0.08 M oxalic acid. Table 1 lists the functional groups present based on the FTIR spectra of the samples.

The surface morphology of the polymers and the elemental composition of the prepared PANI and GF-PANI were analyzed by FESEM-EDX. Figure 6 shows the FESEM and EDX images of PANI. The weight percentages are shown in Table 2. The FESEM image of the PANI nanocomposite showed spherical and 'cauliflower-like' shapes. This structure can increase light absorption and utilization while also shortening the transfer distance for photogenerated electrons, resulting in strong photocatalytic activity for the hydrogen evolution cycle[24]. The presence of oxygen at 12 wt % in the EDX analysis proved that the PANI backbone contained oxalic acid.

Table 2. Elemental composition of PANI.

Element	Wt%	At%
C	65.70	71.09
N	19.58	18.17
O	12.00	9.75
Cl	2.73	1.00

****

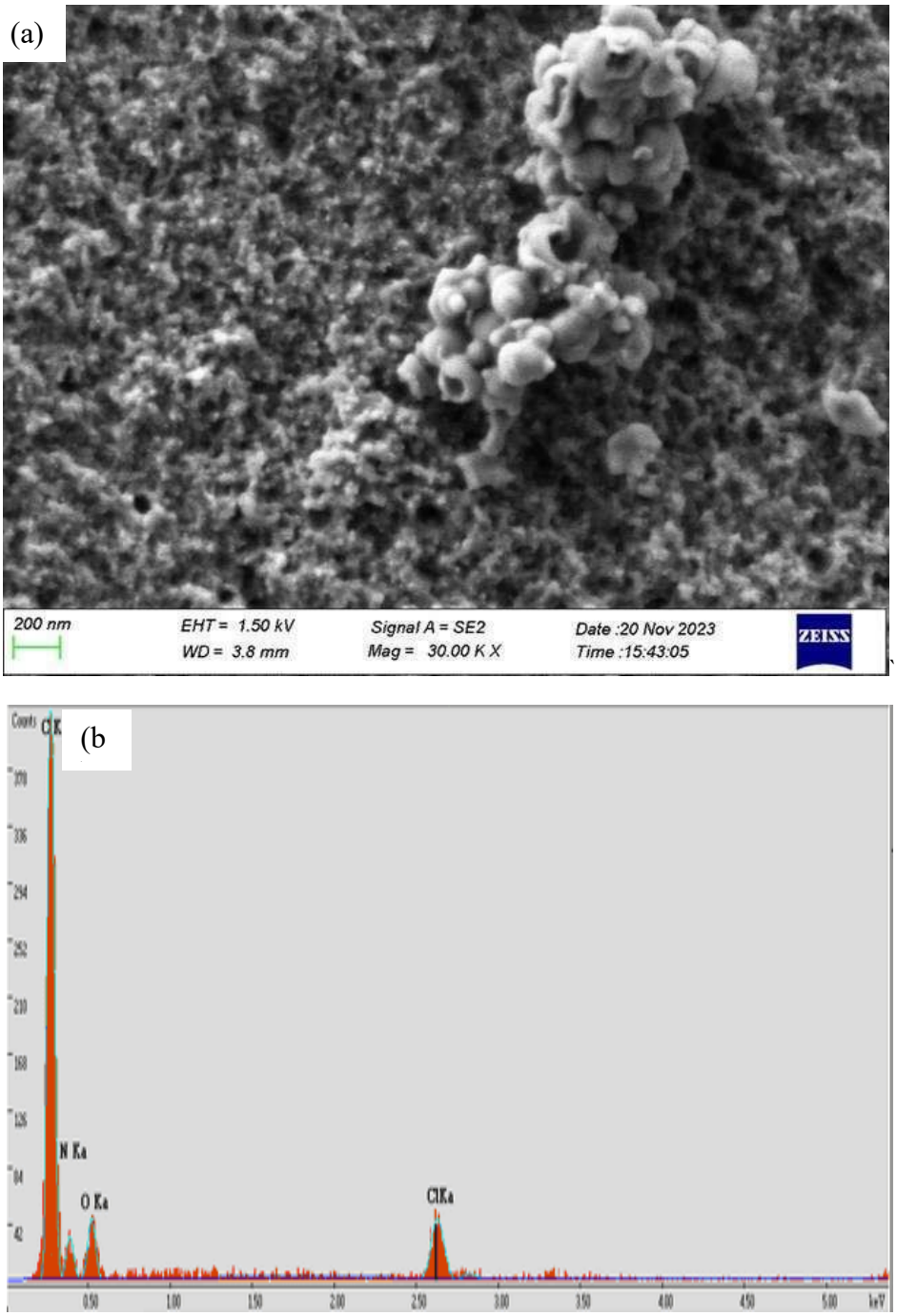

Figure 6. FESEM image (a) and EDX spectrum (b) of PANI with 0.08 M oxalic acid.

Figure 7 demonstrates the micrographs of the graphite felt samples (unmodified, modified, and carbonized modified GF). The unmodified GF exhibited fibres with a smooth surface, while the modified GF with PANI showed that PANI was uniformly coated on the GF fibres. The carbonized modified GF showed a porosity in the fibres after being carbonized in the furnace for 2 hours at 400 °C. The deoxidation of oxygen-containing functional groups during carbonization of the modified GF-PANI composite led to the formation of a mesoporous structure, as confirmed by the BET analysis shown in Figure 8(a) and (b). The mesoporous structure has the advantage that it may interact with molecules, atoms, ions, and nanoparticles on the surface, as well as with the material itself, making it ideal for accelerated adsorption reactions [25]. Mesoporous structures have higher pore volumes and active sites, which lead to higher adsorption. The porosity of electrode materials for energy devices is important due to the demand for high electronic conductivity for better performance. The high porosity provides a more active site for the reaction.

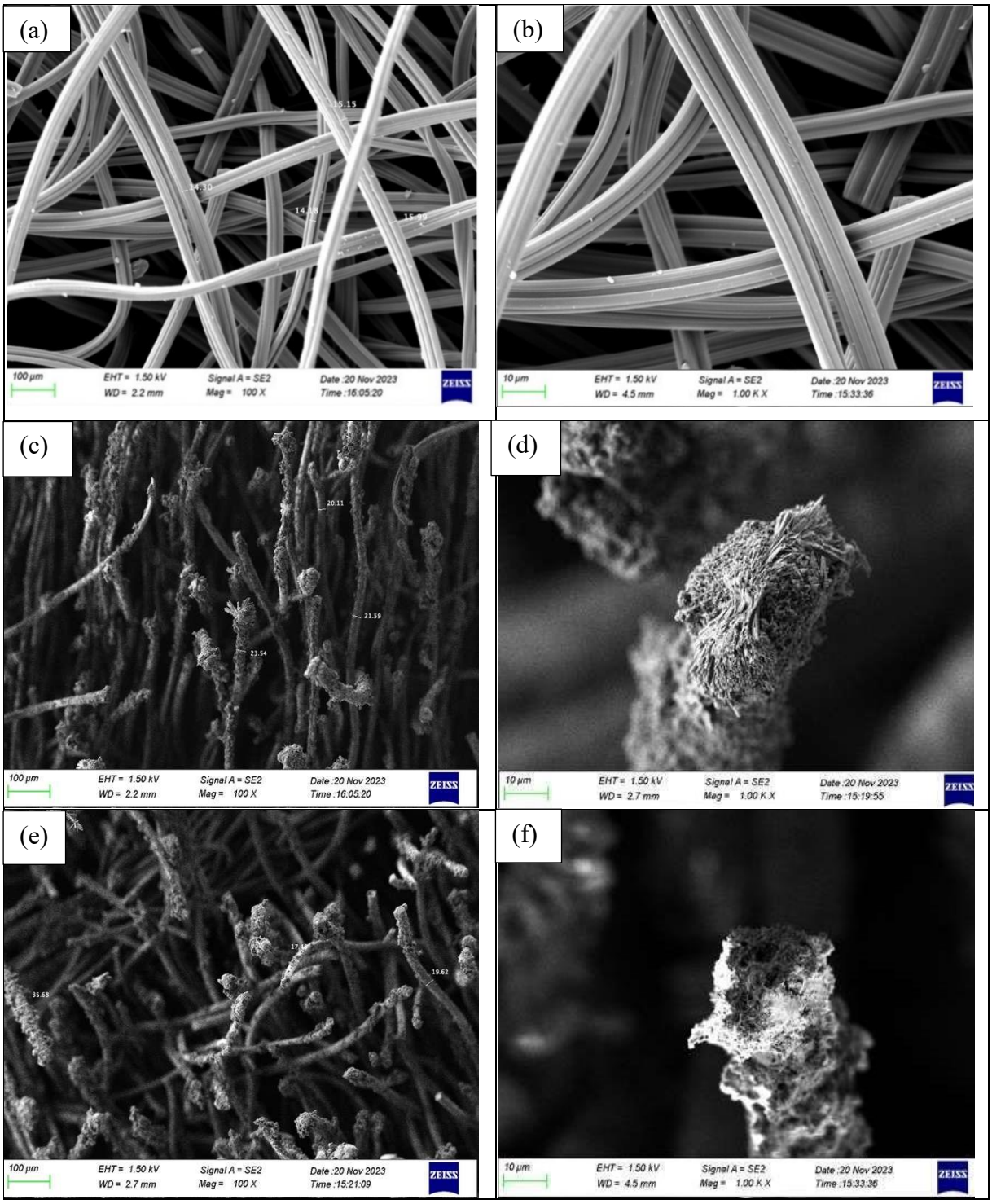

Figure 7. FESEM images of unmodified GF (a-b), modified GF-PANI (c-d), and carbonized modified GF-PANI (e-f).

Figure 8(a) and (b) demonstrated the results of a BET analysis of GF materials across modification and carbonization.

The nitrogen adsorption–desorption and pore size distribution data (Figure 8(a)) offer a clear view of the progressive structural transformation of graphene fibre (GF) materials through polyaniline (PANI) modification and subsequent carbonization. Three distinct samples were analysed: unmodified GF, modified GF-PANI (before carbonization), and carbonized modified GF-PANI. The BET surface area provides crucial insights into the availability of surface-active sites, which are particularly relevant for applications involving electrochemical reactions or adsorption processes. To evaluate the pore size

distribution and average pore diameter values, the Barret-Joyner-Halenda (BJH) method was used, which derives information from the desorption branch of the isotherm. This method is especially suited for analysing mesoporous structures (2-50 nm) by applying the Kelvin equation, which relates the relative pressure of gas adsorption to the radius of curvature of the liquid meniscus in the pores. The resulting data include total pore volume, average pore diameter and a pore size distribution curve, all of which are essential in determining how effectively the material can allow ion transport or host active species.

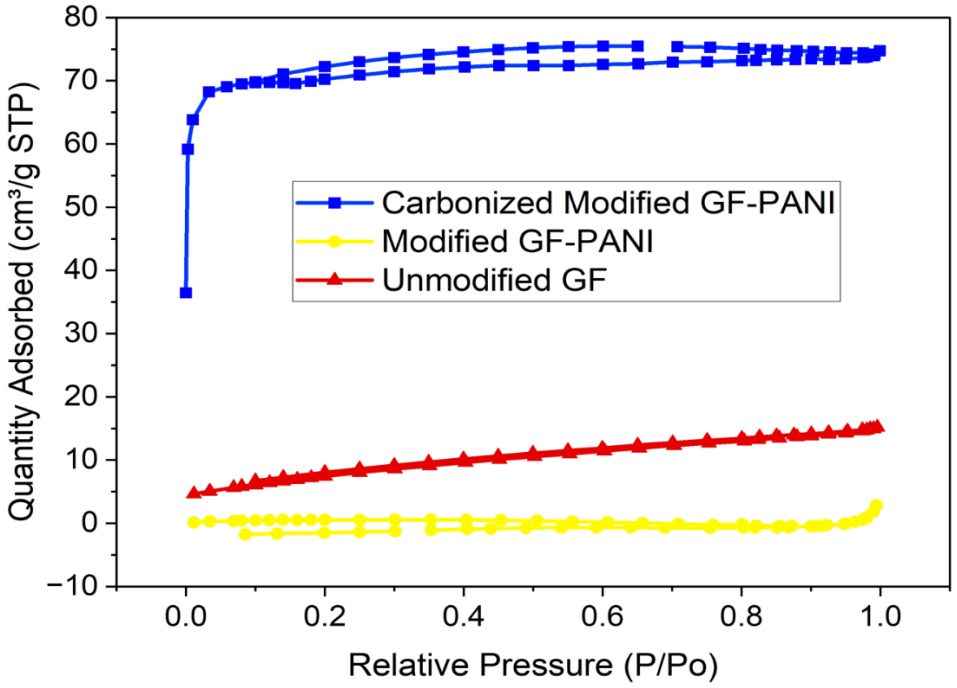

Figure 8(a). The nitrogen adsorption-desorption isotherm of unmodified GF, modified GF-PANI and carbonized modified GF-PANI.

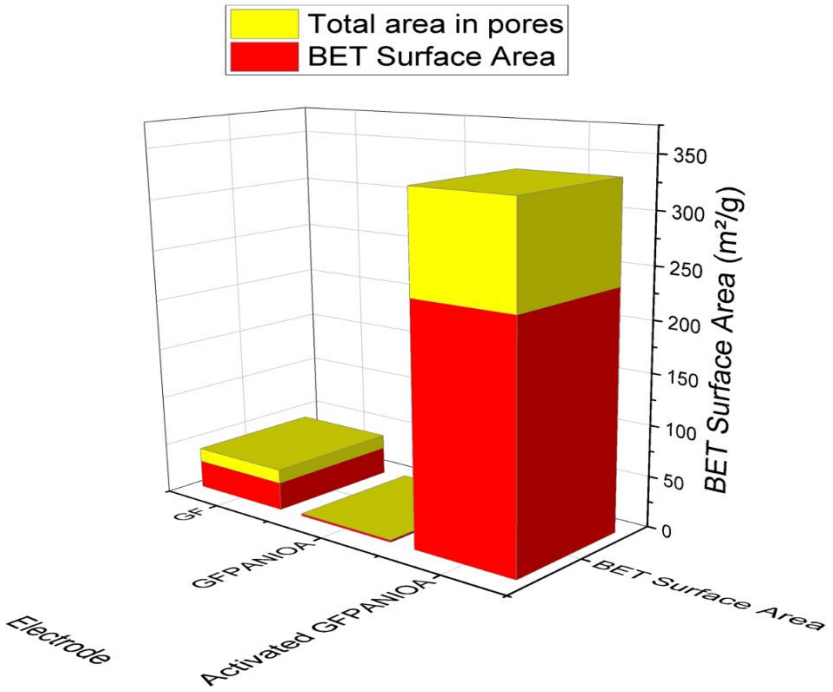

Figure 8(b). BET surface area and total area from pore analysis of unmodified GF, modified GF-PANI and carbonized modified GF-PANI.

Table 3. BET surface area, total pore volume, BJH pore size and DFT surface area data for unmodified GF, modified GF-PANI and carbonized modified GF-PANI.

Sample	BET Surface Area (m^2/g)	Total Pore Volume (cm^3/g)	BJH Pore Size (nm)	DFT Surface Area(m^2/g)
Unmodified GF	27.46	0.022	3.75	13.55
Modified GF-PANI	2.13	0.0019	17.26	0.064
Carbonized Modified GF-PANI	234.19	0.115	2.84	97.72

To obtain a more accurate pore size distribution, particularly in the micro and mesopore range, Density Functional Theory (DFT) analysis was performed. Unlike classical methods, DFT is based on statistical thermodynamics and simulates the adsorption behaviour of nitrogen gas in model pores of varying geometries. This method provides high-resolution data on pore volume, surface area and distribution, especially for samples with pore sizes less than 2 nm that are not reliably resolved by BJH analysis. DFT is used for a comprehensive understanding of the material's porosity.

The unmodified GF sample exhibited a moderate BET surface area of 27.46 m^2/g, with a total pore volume of 0.02195 cm^3/g, and an average BJH pore diameter of 3.75 nm (Table 3). These values indicate some intrinsic mesoporosity, but the overall surface area and pore connectivity were limited, restricting potential electrochemical performance. After PANI modification (prior to carbonization), a dramatic decrease in surface area was observed: the BET surface area dropped to just 2.13 m^2/g, and the total pore volume fell to 0.00193 cm^3/g. The BJH pore size distribution shifted drastically, with very large average diameters (17.26 nm adsorption, 94.97 nm desorption) indicating the presence of less efficient or collapsed pores likely due to PANI coating the GF surface and filling preexisting pores. The extremely low DFT surface area (0.064 m^2/g) suggested a loss of accessible porosity at this stage. This drop is common when non-carbonized polymer coatings block diffusion pathways.

However, upon carbonization and activation, the material transformed significantly. The BET surface area rose steeply to 234.19 m^2/g, the Langmuir surface area to 304.63 m^2/g, and the total pore volume increased over 60 times compared to the PANI-coated sample. Additionally, the average mesopore diameter narrowed to ~2.27–2.84 nm, with a well-defined pore structure ideal for electrolyte infiltration and ion diffusion. These findings demonstrate that carbonization not only restored but substantially enhanced the porosity of the GF-PANI system. This is likely due to the thermal decomposition of PANI, which introduced new mesopores and exposed previously blocked sites, while the graphene fibre backbone retained structural integrity and conductivity [26]. The result was a highly porous, high-surface-area material with a stable framework, optimal for electrochemical energy applications such as supercapacitors or batteries.

Electrochemical Impedance Spectroscopy (EIS) is used to analyse the properties of materials and electrode reactions. More impedance values that demonstrate the impact of mass transport and response mechanics are highlighted by the Nyquist representation. When the resistor received most of the current, electrochemical impedance spectroscopy was used to produce the Nyquist plot semicircle. As the real resistor, Z_{real}, increases, the total imaginary component, $Z_{Imaginary}$, will decrease. In this scenario, a semicircle is guided by an ideal capacitor in parallel with a resistor. Simultaneously, the resistor functions as a charge transfer resistance, which prevents the electron from shifting its phase from the electrode into the membrane. Figure 9 below shows an equivalent circuit to fit the electrochemical impedance spectroscopy (EIS) data.

The electrochemical impedance spectra of the unmodified GF, modified GF-PANI, and carbonized modified-PANI electrodes were fitted using the equivalent circuit model comprising an electrolyte resistance (Rs) in series with two parallel branches: one branch containing the double-layer capacitance (Cdl) and another containing the charge transfer resistance (Rct) and Warburg impedance (W) elements. Based on the fitting results shown in Table 4, modification of GF with PANI reduced the Rs value, indicating improved ionic conductivity of the electrolyte at the electrode interface. The dramatic decrease in Rct after carbonization reflects enhanced electron transfer kinetics across the electrode surface, consistent with the increase in electrical conductivity from 0.0043 S cm^{-1} to 0.0214 S cm^{-1}. The Warburg element (W) also showed lower impedance after modification, suggesting faster ion diffusion processes. These results confirm that the fitted circuit parameters (lower Rs, Rct, and W) aligned with the improved electrochemical properties of the PANI-modified and carbonized GF electrodes. Similar findings have been reported in previous studies, where PANI-based modifications significantly reduced charge transfer

resistance (Rct) and solution resistance (Rs), leading to enhanced ion transport and conductivity at the electrode-electrolyte interface [27-29]. As summarized in Table 5, the PANI-based surface modification achieved superior charge transfer characteristics compared to other treatment methods, validating the effectiveness of this approach based on the fitted circuit model.

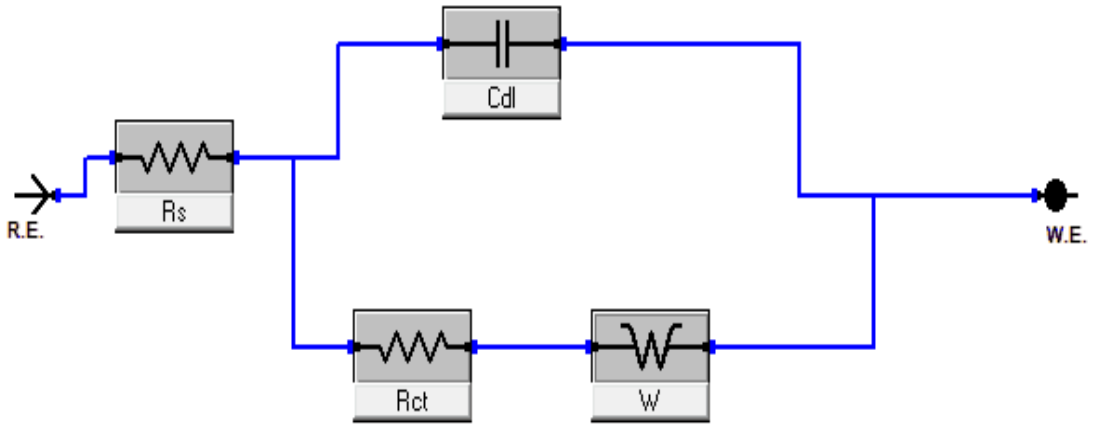

Figure 9. Equivalent circuit fit in electrochemical impedance spectroscopy.

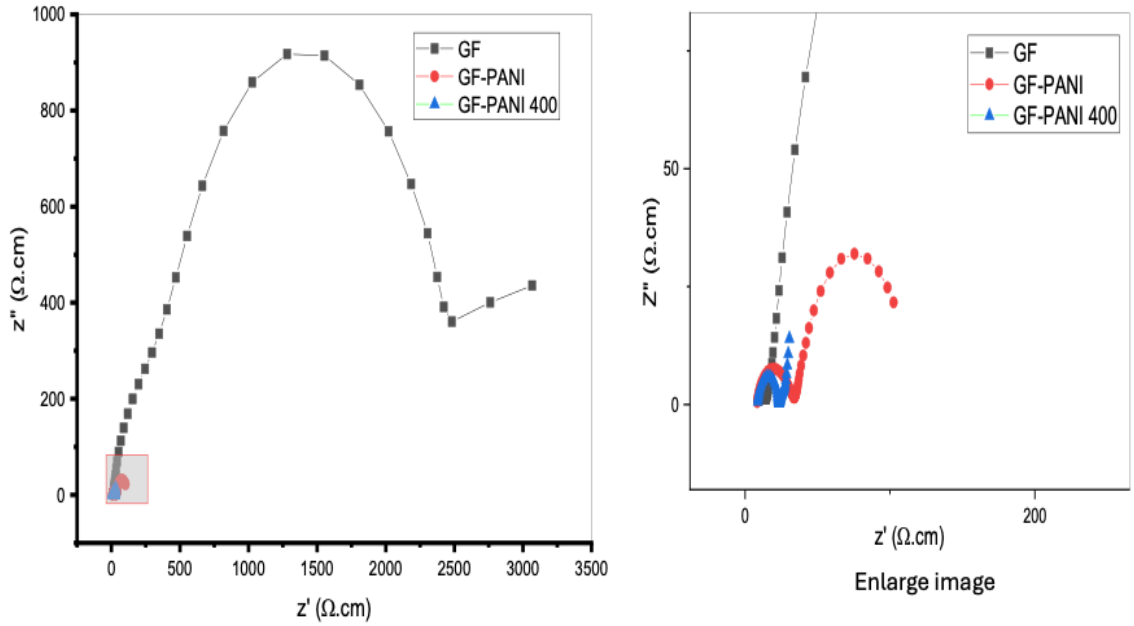

Figure 10. The electrochemical impedance spectroscopy results for unmodified GF, modified GF-PANI and carbonized GF-PANI.

Table 4. Rs, Rct and conductivity values for unmodified GF, modified GF-PANI and carbonized GF-PANI.

Sample	Rs (Ω)	Rct (Ω)	Conductivity σ (Scm^{-1})
GF	9.54	116.18	0.0043
Modified GF-PANI	8.39	34.02	0.0147
Carbonized GF-PANI	8.79	23.36	0.0214

Table 5. Comparison with other modification methods.

Modification method	Rct(Ω)	Conductivity (Scm^{-1})	Key Benefits
Unmodified GF	116.18	0.0043	Poor electron transport
Thermally Treated GF	~40-60 [4]	~0.01 [4]	Moderate charge transfer improvement
Acid-treated GF	~30-50 [14]	~0.015 [14]	Increased surface functional groups
N-doped GF	~25-35 [10]	~0.018 [10]	Enhanced electrochemical activity
GF-PANI (this study)	23.36	0.0214	High conductivity & excellent charge transfer

This suggests that modification of GF with oxalic acid-doped PANI enhances electronic conductivity and facilitates ion diffusion at the electrode-electrolyte interface. The influence of a lower Rct will directly improve the electrical conductivity of the modified GF with PANI from 0.0043 S cm^{-1} to 0.0214 S cm^{-1}, as evaluated by EIS. The presence of conducting PANI chains with quinonoid and benzenoid structures facilitates efficient electron delocalization, improving the electrode's electrical properties [30].

Cyclic voltammetry (CV) is a technique to analyse electron transfer mechanisms in the electrode by measuring the resulting current. Figure 11 illustrates the CV curve for unmodified GF and carbonized modified GF-PANI at 10 mV s^{-1} in 1 M H_2SO_4 electrolyte. The unmodified GF showed an oxidative peak at 1.22 V and a reductive peak at 0.404 V. The carbonized modified GF-PANI showed a pseudocapacitive curve with a wide voltage range from -0.19 V to a maximum of 1.5 V. The well-defined redox peaks suggest efficient electron transfer and improved electrochemical reversibility, which are attributed to the conducting PANI layer. The area in the CV curve shows the conductivity of the electrode. A bigger area can be observed in the carbonized modified GF-PANI electrode, thus its conductivity is higher than that of the unmodified GF. This indicates enhanced charge storage capability, a result of improved electrode conductivity and higher surface area. The pseudocapacitive behaviour is electrochemically reversible over an extended time, with no mass transfer limitation [31].

Figure 12 shows the CV curve at multiple scan rates from 5 mV s^{-1} to 100 mV s^{-1}. By increasing the scan rate, the current flow increased in the system. As the scan rate increased, the oxidation and reduction peak currents increased, demonstrating fast charge transfer kinetics and good reversibility. The peak separation remained relatively small, indicating low internal resistance and a more stable redox reaction. The linear relationship between the peak current and the square root of the scan rate suggests a diffusion-controlled electrochemical process, further confirming the excellent ion transport capability of the modified electrode [32].

The specific capacitance of the carbonized modified GF-PANI electrode was determined through cyclic voltammetry (CV) at a scan rate of 10 mV s^{-1} in 1 M H_2SO_4. With an active material mass of 2 mg cm^{-2}, the calculated specific capacitance was approximately 125 F g^{-1}. This value is indicative of the pseudocapacitive behaviour arising from the redox activity of polyaniline, as well as the enhanced ion transport facilitated by the mesoporous structure formed during carbonization. The improved electrochemical performance of the oxalic acid-doped PANI GF electrode is comparable to other conductive polymer-modified electrodes [14, 18, 33]. Research has suggested that the specific capacitance of a material must be in the range of 100- 300 F g^{-1} to perform as a good supercapacitor [34].

The cyclic voltammetry (CV) analysis revealed clear redox peaks for the carbonized GF-PANI electrode, indicative of its pseudocapacitive behaviour and efficient charge transfer kinetics. The enhanced current response compared to unmodified GF highlights the improved electrochemical activity facilitated by the conductive PANI network and the increased surface area achieved through carbonization. These characteristics contribute directly to its specific capacitance, which was calculated to be 125 F g^{-1} at a scan rate of 10 mV s^{-1}. This capacitance value aligns well with typical PANI-modified graphite felt electrodes, demonstrating its competitive performance while also offering significant advantages in terms of mechanical stability and ionic conductivity. The carbonization process not only preserved the electrode's electrochemical properties but also enhanced its robustness, addressing common limitations such as polymer swelling and structural degradation. Consequently, the carbonized GF-PANI electrode is poised to deliver reliable and stable performance in vanadium redox flow battery (VRFB) applications, where long-term cycling and durability are critical.

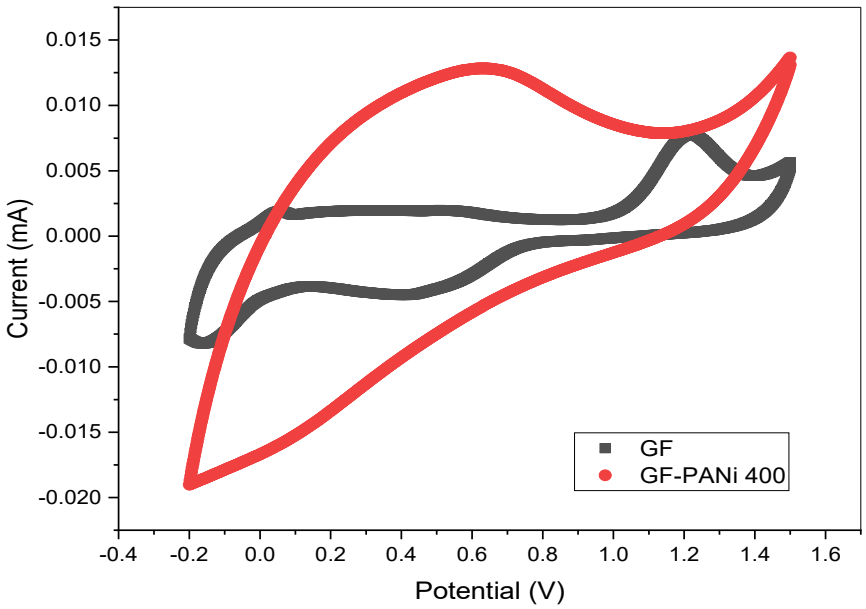

Figure 11. CV curves for unmodified GF and carbonized modified GF-PANI at 10 mVs^{-1}.

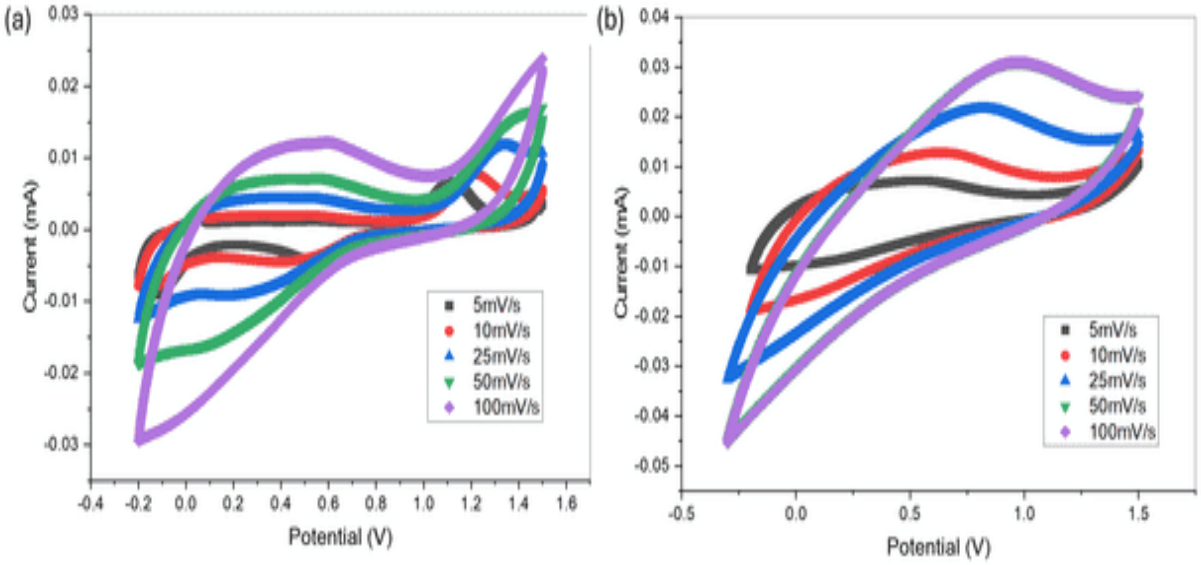

Figure 12. CV curves for unmodified GF (a) and carbonized GF-PANI (b) at various scan rates.

From the CV curve, the power density was calculated based on the average power density (P) equation below:

$$P = \frac{E^2}{4R} \quad (6)$$

Applying specific capacitance and assuming ideal behaviour:

$$P = \frac{1}{2} C_s V^2 \quad (7)$$

where P is the power density (W g^{-1}), C_s is specific capacitance (F g^{-1}), and V is the potential window (V).

Hence, the approximate power density of the carbonized modified GF-PANI electrode, calculated from the cyclic voltammetry data, was 178.5 W g^{-1}. This high value reflects the excellent capability of the electrode to deliver rapid energy output, attributable to the combination of enhanced electrical conductivity (0.0214 S cm^{-1}) and the highly porous mesostructure developed during carbonization. In comparison, a modified graphite felt electrode for an MV/4-HO-TEMPO flow battery, reported by Li, X. & Huang, C. (2020), achieved a power density of approximately 110 mW cm^{-2}, highlighting the effectiveness of electrode surface modification [35]. Another study

demonstrated that graphite felt electrodes modified with binary $NiCoO_2$ exhibited enhanced electrochemical performance in vanadium redox flow batteries, with improved voltage efficiency and discharge capacity [33]. The power density value of the carbonized modified GF-PANI electrode obtained in the current study suggests comparable or even superior performance, particularly considering the benefits of enhanced conductivity, high surface area, and pseudocapacitive behaviour tailored for aqueous vanadium redox flow systems.

CONCLUSION

This study effectively created a high-performance GF electrode by modifying it with oxalic acid-doped polyaniline via oxidative polymerization. The addition of oxalic acid markedly improved the conductivity and electrochemical activity of the electrode, as demonstrated by FTIR analysis, which verified the existence of the essential functional groups responsible for charge transport.

The FESEM images showed GF fibres with a well-coated, porous structure, which enhanced the active surface area and promoted improved electrolyte interaction. EDX results confirmed the presence of oxygen due to oxalic acid doping, hence validating the structural alterations. The carbonization procedure enhanced porosity, essential for effective ion diffusion and electrochemical processes.

Electrochemical analysis revealed that the modified GF-PANI electrode had reduced charge transfer resistance (Rct), increased conductivity, and improved pseudocapacitive behaviour, with a specific capacitance of 125 F g^{-1} and a high power density value of 178.5 W g^{-1}, rendering it extremely suitable for VRFB applications. The notable enhancement in ion transport kinetics and reaction efficiency indicated that this modified electrode may aid in the development of more efficient and reliable energy storage devices. The findings underscore the promise of oxalic acid-doped PANI as an economical and scalable approach for electrode modification in advanced energy storage technologies.

ACKNOWLEDGEMENTS

This work was supported by the 'Geran Insentif Penyeliaan' (GIP) by Universiti Teknologi Mara (UiTM). The authors would like to acknowledge Universiti Teknologi MARA for providing designated labs and facilities for the research.

REFERENCES

1. Gielen, D., Boshell, F., Saygin, D., Bazilian, M. D., Wagner, N. and Gorini, R. (2019) The role of renewable energy in the global energy transformation. *Energy Strategy Reviews*, **24**, 38-50.

2. Kebede, A. A., Kalogiannis, T., Van Mierlo, J. and Berecibar, M. (2022) A comprehensive review of stationary energy storage devices for large scale renewable energy sources grid integration. *Renewable and Sustainable Energy Reviews*, **159**, 112213.

3. Zhong, S., Padeste C., Kazacos, M. and Skyllas-Kazacos, M. (1993) Comparison of the physical, chemical and electrochemical properties of rayon- and polyacrylonitrile-based graphite felt electrodes. *Journal of Power Sources*, **45**, 29–41.

4. Sun, B. and Skyllas-Kazacos, M. (1992) Modification of graphite electrode materials for vanadium redox flow battery application—I. *Thermal treatment. Electrochimica Acta*, **37(7)**, 1253–1260.

5. Bayeh, A. W., Kabtamu, D. M., Chang Y. -C., Chen, G. -C., Chen, H. -Y., Liu, T. -R., Wang, C. -H. (2019) Hydrogen-Treated Defect-Rich W18O49 Nanowire-Modified Graphite Felt as High-Performance Electrode for Vanadium Redox Flow Battery. *ACS Applied Energy Materials*, **2(4)**, 2541–2551.

6. Mohanty, D., Wang, Y. -H., Tsai, Y. -C. and Hung, I. M. (2024) Reprint of "Characteristics and electrochemical performance of copper/graphite felt composite electrodes for vanadium redox flow battery". *Journal of the Taiwan Institute of Chemical Engineers*, **154**, 105316.

7. Wang, L., Li, S., Li, D., Xiao, Q. and Jing, W. (2020) 3D flower-like molybdenum disulfide modified graphite felt as a positive material for vanadium redox flow batteries. *RSC Advances*, **10(29)**, 17235–17246.

8. Hassan, A. and Tzedakis, T. (2019) Enhancement of the electrochemical activity of a commercial graphite felt for vanadium redox flow battery (VRFB), by chemical treatment with acidic solution of K2Cr2O7. *Journal of Energy Storage*, **26**, 100967.

9. Piwek, J., Gonzalez, G., Peljo, P. and Frackowiak, E. (2023) Molten salt carbon felt oxidation for VRFB electrode performance improvement. *Carbon*, **215**, 118483.

10. Chen, X., Wu, C., Lv, Y., Zhang, S., Jiang, Y., Feng, Z., He, Z. (2025) Highly active nitrogen-phosphorus co-doped carbon fiber@graphite felt electrode for high-performance vanadium redox flow battery. *Journal of Colloid and Interface Science*, **677**, 683–691.

11. Hsiao, Y. -S., Huang, J. -H., Lin, H. -Y., Pang, W. K., Hung, M. -T., Cheng, T. -H., Huang, Y. -C.

(2024) Surface-modified graphite felt incorporating synergistic effects of TiO2 decoration, nitrogen doping, and porous structure for high-performance vanadium redox flow batteries. *Surface and Coatings Technology*, **484**, 130785.

12. Liu, W. -F., Kim, K. -H. and Ahn, H. -J. (2023) NTO laminated graphite felt as high-performance negative electrode for vanadium redox flow batteries. *Journal of Alloys and Compounds*, **954**, 170106.

13. Jeon, S., An, H., Noh, C., Kwon, Y. and Chung, Y. (2023) Green surface treatment of graphite felt using modified TEMPO mediated oxidation for use in vanadium redox flow batteries. *Applied Surface Science*, **613**, 155962.

14. Wu, X., Xie, Z., Zhou, H., Xiong, Z. A., Yin, X., Tang, H., Liao, J. (2023) Designing high efficiency graphite felt electrode via HNO3 vapor activation towards stable vanadium redox flow battery. *Electrochimica Acta*, **440**, 141728.

15. Wang, H., Lin, J. and Shen, Z. X. (2016) Polyaniline (PANi) based electrode materials for energy storage and conversion. *Journal of Science: Advanced Materials and Devices*, **1(3)**, 225–255.

16. Dhawale, D., Vinu, A. and Lokhande, C. (2011) Stable nanostructured polyaniline electrode for supercapacitor application. *Electrochimica Acta*, **56(25)**, 9482–9487.

17. Simotwo, S. K. and Kalra, V. (2016) Polyaniline-based electrodes: recent application in super-capacitors and next generation rechargeable batteries. *Current Opinion in Chemical Engineering*, **13**, 150–160.

18. U, R., Mohan, S., Revanasiddappa, M. and Vellakkat, M. (2023) Conducting polymer/ transition metal carbide nanocomposite treated graphite felt as positive electrode in all-vanadium redox flow battery. *Synthetic Metals*, **294**, 117311.

19. Li, Z. and Gong, L. (2020) Research Progress on Applications of Polyaniline (PANI) for Electrochemical Energy Storage and Conversion. *Materials (Basel, Switzerland)*, **13.** E548 DOI: 10.3390/ma13030548.

20. Jiang, X., Lou, S., Chen, D., Shen, J., Han, W., Sun, X., Wang, L. (2015) Fabrication of polyaniline/ graphene oxide composite for graphite felt electrode modification and its performance in the bioelectrochemical system. *Journal of Electroanalytical Chemistry*, **744**, 95–100.

21. Bednarczyk, K., Matysiak, W., Tański, T., Janeczek, H., Schab-Balcerzak, E. and Libera, M. (2021) Effect of polyaniline content and protonating dopants on electroconductive composites. *Scientific Reports*, **11(1)**, 7487.

22. Balakrishnan, D., Pragathiswaran, C., Thanikasalam, K., Mohanta, Y. K., Saravanan, M. and Abdellattif, M. H. (2022) Molecular Docking and In Vitro Inhibitory Effect of Polyaniline (PANI)/ZnO Nanocomposite on the Growth of Struvite Crystal: a Step Towards Control of UTI. *Applied Biochemistry and Biotechnology*, **194(10)**, 4462–4476.

23. Ahmad Tarmizi, A. A., Harun, M. K., Abdullah, S., Bahron, H., Yahya, M. Z. A., Yahaya, S. M. and Abdul Halim, N. H. (2016) The Effect of Oxalic Acid as a Doping Agent on the Conductivity of Polyaniline. *Scientific Research Journal*, **13(1)**, 15–23.

24. Liu, X., Ruan, Z., Zhang, L., Li, Y., Jiang, Y., Fan, J., Lin, K. (2021) Porous cauliflower-like molybdenum disulfide/cadmium sulfide hybrid micro/nano structure: Enhanced visible light absorption ability and photocatalytic activity. *Journal of Colloid and Interface Science*, **590**, 352–364.

25. Han, Z., Wang, T., Cai, Y., Rong, S., Ma, J., Hou, L. and Ji, Y. (2024) Electrospun porous carbon nanofiber-based electrodes for redox flow batteries: Progress and opportunities. *Carbon*, **222**, 118969.

26. Gao, Z., Yang, W., Wang, J., Yan, H., Yao, Y., Ma, J., Liu, L. (2013) Electrochemical synthesis of layer-by-layer reduced graphene oxide sheets/ polyaniline nanofibers composite and its electrochemical performance. *Electrochimica Acta*, **91**, 185–194.

27. Ben, J., Song, Z., Liu, X., Lü, W. and Li, X. (2020) Fabrication and Electrochemical Performance of PVA/CNT/PANI Flexible Films as Electrodes for Supercapacitors. *Nanoscale Research Letters*, **15(1)**, 151.

28. Graves, D. A., Theodoroviez, L. B., de Oliveira, T. C., Cividanes, L. S., Ferreira, N. G., Almeida, D. A. L. and Gonçalves, E. S. (2023) Enhanced electrochemical properties of polyaniline (PANI) films electrodeposited on carbon fiber felt (CFF): Influence of monomer/acid ratio and deposition time parameters in energy storage applications. *Electrochimica Acta*, **454**, 142388.

30. Bhadra, S., Chattopadhyay, S., Singha, N. K. and Khastgir, D. (2008) Improvement of conductivity

of electrochemically synthesized polyaniline. *Journal of Applied Polymer Science*, **108(1)**, 57–64.

31. Fleischmann, S., Mitchell, J. B., Wang, R., Zhan, C., Jiang, D. -E., Presser, V. and Augustyn, V. (2020) Pseudocapacitance: From Fundamental Understanding to High Power Energy Storage Materials. *Chemical Reviews*, **120(14)**, 6738–6782.

32. Kinkelin, S. -J., Röder, F., Vogel, K., Steimecke, M. and Bron, M. (2024) A fundamental study on cyclic voltammetry at porous carbon thin-film electrodes. *Electrochimica Acta*, **488**, 144183.

33. Xiang, Y. and Daoud, W. A. (2019) Binary NiCoO2-modified graphite felt as an advanced positive electrode for vanadium redox flow batteries. *Journal of Materials Chemistry A*, **7(10)**, 5589–5600.

34. Patel, A., Patel, S. K., Singh, R. S. and Patel, R. P. (2024) Review on recent advancements in the role of electrolytes and electrode materials on supercapacitor performances. *Discover Nano*, **19(1)**, 188.

35. Li, X. and Huang, C. (2020) A new modification method for graphite felt electrodes in a MV/4-HO-TEMPO flow battery. *RSC Advances*, **10(11)**, 6333–6341.